KSME

Springer

Journal of Mechanical Science and Technology 34 (8) 2020

Original Article
DOI 10.1007/s12206-020-0720-4

Keywords:
· Boiler tube
· Creep life
· Image analysis
· Precipitate
· Service aging
· Tempered martensite
· T91

Correspondence to:
Kee Bong Yoon
kbyoon@cau.ac.kr

Citation:
Lok, V., Le, T. G., Yu, J. M., Ma, Y. W., Nguyen, V. P., Choi, S. T., Yoon, K. B. (2020). Changes in creep property and precipitates due to aging of T91 steel after long-term service. Journal of Mechanical Science and Technology 34 (8) (2020) 3283~3293.
http://doi.org/10.1007/s12206-020-0720-4

Received April 20th, 2020
Revised May 23rd, 2020
Accepted June 8th, 2020

† Recommended by Editor Chongdu Cho

Changes in creep property and precipitates due to aging of T91 steel after long-term service

Vanno Lok[1], Thi Giang Le[1], Jong Min Yu[1], Young Wha Ma[2], Vinh Phu Nguyen[1], Seung Tae Choi[1] and Kee Bong Yoon[1]

[1]Department of Mechanical Engineering, Chung-Ang University, 84 Heukseok-ro, Dongjak-gu, Seoul 06974, Korea, [2]R&D Institute, Doosan Heavy Industries & Construction, Changwon, Korea

Abstract The creep deformation behavior of virgin and long-term service-aged (77000 h) T91 steel of superheater tubes in a power plant was assessed via creep tests along with microstructure examination. A series of miniature tensile creep tests were conducted at 590 °C under applied stresses ranging from 120.0 to 224.1 MPa for both material types. The creep behavior was examined in terms of variations in the microstructural properties correlated with creep rupture life and ductility. X-ray diffraction, optical microscopy, field-emission scanning electron microscopy, hardness measurements, and image analyses were used to analyze the shape and morphology of the existing δ-ferrite, tempered martensite microstructure, and precipitates in both the virgin and long-term service-aged materials. The presence of larger residual δ-ferrite in the virgin microstructure was one of the causes of creep rupture strength reduction in the virgin material. On the contrary, the synergistic effect of the tempered martensite lath microstructure and additional precipitation strengthening of fine precipitates had beneficial effects translating to retention of the creep rupture strength of the long-term service-aged material.

1. Introduction

Grade 91 martensitic steels were developed owing to the demand for ferritic steels having higher creep strengths. However, to date, such materials have presented limitations with respect to long-term service at elevated temperatures, i.e., for different structural components such as headers, boiler tubes, and steam generators in thermal and nuclear power plants [1-3]. This steel grade has been widely used for steam pipes and tubes in the construction of high-temperature thermal boilers and steam generators for nuclear power plants since the 1980 s, and it was selected as the American Society of Mechanical Engineers (ASME) Code material in 1983 [4]. These steels have demonstrated good performance even under a temperature of 600 °C owing to their excellent creep resistance, high thermal conductivity, low thermal expansion, and good steam corrosion resistance to oxidation cracking [5, 6]. As this class of materials is the one demonstrating an inherently open structure insensitive to void nucleation due to metallurgical factors, these materials are important and suitable for use in high-temperature applications [7].

The Grade 91 steel is produced from 9Cr-1Mo steel upon strict control of the alloy chemical composition and heat treatment optimization. The presence of δ-ferrite phase was reported to reduce the creep rupture strength and intensify solidification cracking in Grade 91 steel [2, 3, 8]. Thus, the Electric Power Research Institute also recommended controlling the chemical composition properly to increase the material performance with respect to creep ductility. Modification of the chemical composition of Grade T91 steel is achieved via the controlled addition of Nb, N, and V [9]. These alloying elements provide precipitation strengthening via the formation of fine MX-type carbonitrides during deformation under the creep condition [10], which is an additional benefit to the existing solid solution strengthening of Cr-Mo conventional steels [4].

Table 1. Chemical composition of T91 materials and ASTM standard (wt. %).

Material	C	Mn	P	S	Si	Cr	Mo	Ni	V	Nb	N
Virgin	0.10	0.35	0.015	0.002	0.45	8.38	0.88	0.08	0.19	0.07	0.05
Long-term service-aged (77000 h)	0.10	0.46	0.015	0.002	0.34	8.34	0.82	0.12	0.17	0.06	0.05
ASTM 213-11a	0.07-0.14	0.30-0.60	≤ 0.02	≤ 0.01	0.20-0.50	8.00-9.50	0.85-1.05	≤ 0.40	0.18-0.25	0.06-0.10	0.03-0.07
Material	Al	Ti	Zr	As	Sb	Sn	Cu	Pb	B	W	Fe
Virgin	0.06	0.005	0.003	-	0.001	-	0.02	0.008	0.04	0.004	Bal.
Long-term service-aged (77000 h)	0.08	0.01	0.003	0.001	-	0.004	0.12	0.004	0.04	0.05	Bal.
ASTM 213-11a	≤ 0.02	≤ 0.01	≤ 0.01	-	-	-	-	-	-	-	Bal.

Thus, the T91 class steels possess improved creep resistance compared to that of the conventional Cr-Mo steels. The improved properties of this material are also attributed to its tempered martensite microstructure rich in primary precipitates, i.e., MX obtained after austenitization (M = V or Nb and X = C or N) and secondary carbides $M_{23}C_6$ (M = Cr, Fe, Mn or Mo) [11].

Long-term service exposure at high temperatures can cause microstructural changes such as precipitate coarsening, formation of new phases, precipitation, and segregation of some main alloying elements at prior austenite grain boundaries (PAGBs). The segregation occurs mainly at the PAGBs rather than within the grain, which causes weakening of the grain boundaries. However, the segregation can be delayed via application of suitable heat treatments; even so, it cannot be completely avoided during long-term field exposure. The microstructural changes are also due to the coarsening of finely dispersed precipitates along the boundaries via diminishing of the lath structure and diffusion to a new state such as a coarsening precipitate upon absorption of matrix elements [12, 13].

Numerous factors can cause early cracking of Grade 91 steel components during service. The chemical composition can also be a factor responsible for induction of failure early in the operating life due to improper heat treatment of the components. The presence of trace elements and other metallurgical risk factors, such as nonmetallic inclusions or evolution of the Laves phase, can result in void nucleation at the PAGBs or lath boundaries [14]. However, the Laves phase can also strengthen the creep resistance by limiting the deformation of grains and sub-grains, thereby offsetting the loss brought about upon solid solution hardening [15, 16].

Therefore, an understanding of the creep property and microstructural changes during thermal exposure is necessary to assess the stability and performance of T91 steel to enable its effective use in industrial applications. This study aimed to investigate the relationship between the creep strength and microstructural evolution of T91 steel following long-term service. In addition, the effect of the existence of δ-ferrite in the initial microstructure on the creep strength of this material was also discussed.

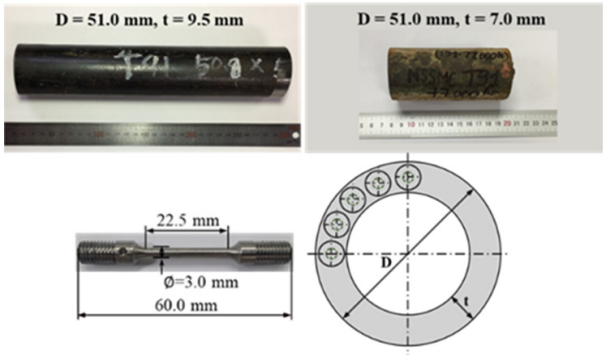

Fig. 1. T91 tubes and miniature creep specimens used in this study.

2. Experimental procedures

2.1 Service-aged superheater tubes and specimens

As mentioned earlier, 9Cr steel was used in the study. T91 steel tubes having undergone two different service conditions were obtained from the superheater of a domestic fossil power plant, as shown in Fig. 1. One tube was in the virgin condition (virgin), and the other had undergone 77000 h of service at 540–590 °C and under 17.3 MPa (long-term service-aged). The tensile properties of the virgin material were as follows: the yield strength, tensile strength, and percent elongation were 526 MPa, 657 MPa, and 42 %, respectively. These tensile properties satisfy the requirements of the T91 material according to the ASTM A213 standard.

For the long-term service-aged T91 tube material, the tensile properties could not be measured because the tube (see Fig. 1) was extremely thin. Instead, the Vickers hardness was measured for both the virgin and the long-term service-aged materials. The hardness of the virgin material was 224.7 HV, and that of the long-term service-aged material was 230.6 HV. From the hardness measurement results, it can be inferred that the tensile strength of the long-term service-aged material was not reduced at all; rather, it had increased by 2.6 % when compared with that of the virgin material.

Table 2. Creep test conditions and measured creep rupture life, reduction of area, and elongation of T91 steel at 590 °C.

Specimen	Applied stress (MPa)	Rupture time (h)	Min. creep strain rate (% h^{-1})	Reduction of area (%)		Elongation (%)	
				Result	Avg.	Result	Avg.
Virgin	166.5	7396.4	5.00E-04	74.33	86.32	16.76	20.77
	201.2	697.7	6.20E-03	89.55		21.29	
	208.1	60.2	7.73E-02	90.18		21.47	
	222.0	20.7	2.82E-01	91.20		23.56	
Long-term service-aged (77000 h)	120.0	Interrupted	-	-	-	-	-
	200.1	881.2	5.60E-03	90.39	90.90	20.00	22.88
	208.1	274.7	1.84E-02	90.60		23.33	
	217.1	233.2	2.31E-02	91.20		26.18	
	224.1	139.7	3.61E-02	91.40		22.00	

2.2 Miniature creep test

Creep tests for nine specimens of the virgin and long-term service-aged T91 materials were conducted at a temperature of 590 °C under applied stresses in the range of 120.0-224.1 MPa. The specimens tested at 166.5-224.1 MPa were reached the rupture and all the three creep stages could be recognized; however, the creep stage of the specimens tested at 120.0 MPa was not reached, as the test is still underway. The test temperature exercised was the same as the service temperature. To prevent oxidation during high-temperature testing, Ar gas was supplied to the furnace. The displacement of the end of a pull rod, which was attached to the miniature specimen, was measured using a linear variable differential transformer with a 1-μm resolution. The creep tests were performed according to the ASTM E139 standard [17]; all the creep test conditions exercised are summarized in Table 2. Creep deformation curves, which indicated the creep strain as a function of elapsed time, were obtained for various stress levels. The reduction of area and percent elongation were measured by fitting the ends of the fractured parts of the specimen as per the ASTM E139 standard [17].

2.3 Microstructural observation

Specimens with dimensions of 10 mm × 10 mm × 0.5 mm were obtained from the cross-sections of the virgin and long-term service-aged T91 materials. For examining the microstructure, these specimens were prepared via standard polishing and etched using Vilella's reagent (solution containing 1 g of picric acid, 5 mL of HCl, and 100 mL of ethanol) for approximately 20 s. Optical microscopy (OM) and field-emission scanning electron microscopy (FE-SEM) were used to investigate the microstructural changes after long-term service. The composition of precipitates was analyzed using energy-dispersive X-ray spectroscopy (EDS) along with FE-SEM. These techniques were also used to map regions containing a particular precipitate. X-ray diffraction (XRD), with CuKα radiation (λ = 0.1541 nm) in the 2θ range from 20 to 90°, was carried out to identify the phase constitution. The database of the Joint Committee on Powder Diffraction Standards (JCPDS) was used as the basis for the phase identification of the crystalline phase via their XRD patterns.

A 54 μm × 36 μm area in the FE-SEM images was used to determine the number, area fraction, and size distribution of precipitates using the ImageJ software (National Institutes of Health, USA) after binarization of each image into black and white [15, 18-20]. To determine the measured precipitate size distributions, the ImageJ software was applied to calculate the areas of the particles in the FE-SEM images, following which the particle areas were converted into equivalent diameters [20-23].

3. Results and discussion

3.1 Creep test results

The creep test results are listed in Table 2 and depicted in Fig. 2. Fig. 2 shows the curves of creep strain versus time for various stresses at 590 °C for the virgin and long-term service-aged materials. For a constant temperature of 590 °C and different stress levels, the creep deformation of T91 steel is characterized typically by a negligible instantaneous loading strain, small transient creep strain, and secondary creep followed by a prolonged tertiary creep regime. The accumulation of strain in the tertiary creep is considerable compared to that in the primary and secondary creep stages, and a rapid creep strain accumulation is observed because of necking just prior to fracture, as indicated in Fig. 2. These creep strain data were converted into creep strain rate data according to the seven-point incremental polynomial method of ASTM E647 [24] (see Fig. 3) on a log-log scale. All the creep curves obtained in this study showed three distinct stages, namely, primary, secondary, and tertiary stages, which are generally obtained in typical creep tests. The primary creep stage was characterized by a systematic decrease in creep strain rate with time, followed which the secondary creep stage was characterized by a minimum creep strain rate. A rapid increase in the creep strain rate was observed for the tertiary creep stage. It is well known that the rate of creep deformation is determined based on the balance between the strain hardening and recovery process es-

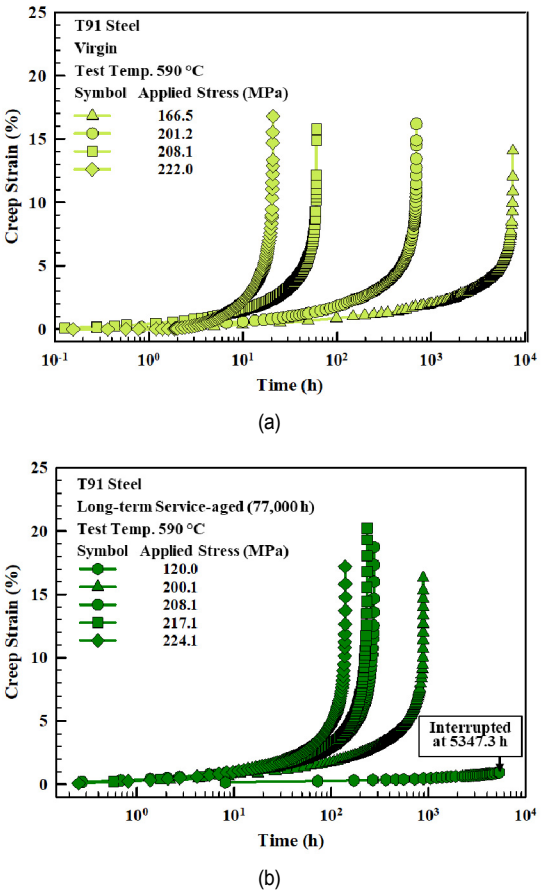

Fig. 2. Creep strain versus time of (a) virgin; (b) long-term service-aged (77000 h) T91 steel materials at 590 °C.

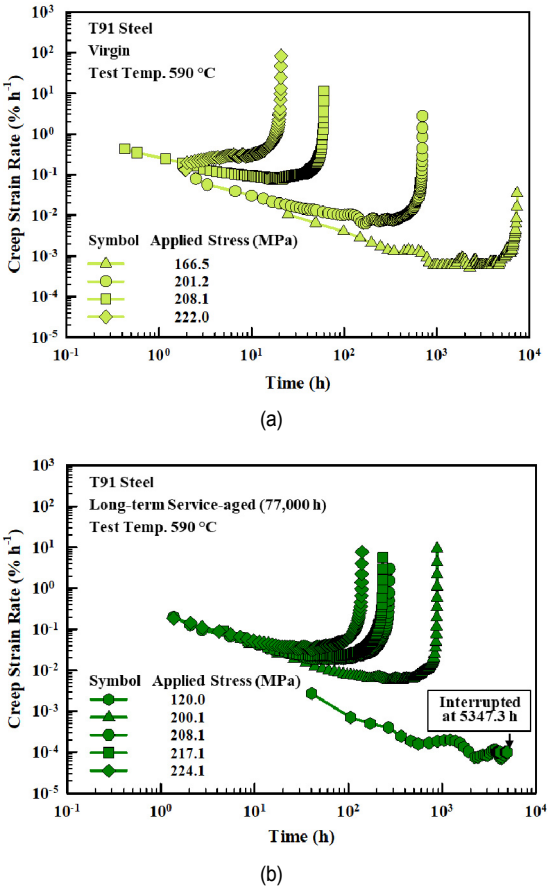

Fig. 3. Creep strain rate versus time of (a) virgin; (b) long-term service-aged (77000 h) T91 steel materials at 590 °C.

tablished during the secondary creep stage [25]. Fig. 3 illustrates the effect of applied stress on the creep strain rate at 590 °C. The minimum creep strain rate increased, but the rupture life decreased with increasing applied stress for both the virgin and long-term service-aged materials.

The relationship between the minimum creep strain rate ($\dot{\varepsilon}$) and the applied stress (σ) was described by Norton's power law creep constitutive equation as expressed in Eq. (1):

$$\dot{\varepsilon} = A\sigma^n \tag{1}$$

where A and n are the power law creep coefficient and creep exponent, respectively. A linear regression line was fitted to the data for both materials, as exhibited in Fig. 4. The value of the creep exponent (n) was determined via the slope of the regression line, and the creep coefficient (A) was determined via the intersection between the regression line and the vertical axis. The estimated values of these creep constants are presented in Table 3 and Fig. 4. The creep exponent values of the virgin and long-term service-aged materials were determined to be 21.636 and 15.253, respectively. The creep exponents *n* in this study are large owing to the high stresses employed. The results suggested that the creep exponent in the high-stress regime is a factor leading to the obstacle of dislocation motion by carbides/nitrides [26].

Fig. 5 displays a comparison of the creep rupture life measured in this study, shown in terms of the Larson-Miller parameter (LMP), and the creep data from the National Institute for Materials Science (NIMS) [27]. The LMP values were determined using Eq. (2):

$$LMP = T(C + \log(t_r)) \tag{2}$$

where T is the temperature (K), C = 28 is the Larson-Miller constant, and t_r is the time to rupture (h). Most of the test data obtained from the virgin and long-term service-aged T91 materials in this study fell within the 99 % error band for Grade 91 steel according to the LMP database [27] in the 550-600 °C temperature range. Generally, it is anticipated that age-induced degradation can lead to a decrease in the creep rupture strength. However, from Fig. 5, it is evident that the long-term service-aged material did not show a reduction in residual creep life. Therefore, it can be stated that the age-induced degradation in the creep rupture strength could be negligible. This can be attributed to the microstructural changes such as the presence of precipitates of much finer distribution, coarsen-

Table 3. Creep coefficient and creep exponent of T91 steel according to Norton's power law for creep.

Specimen	A ($MPa^{-n}.h^{-1}$)	n
Virgin	3.1768×10^{-54}	21.636
Long-term service-aged (77000 h)	5.5634×10^{-40}	15.253

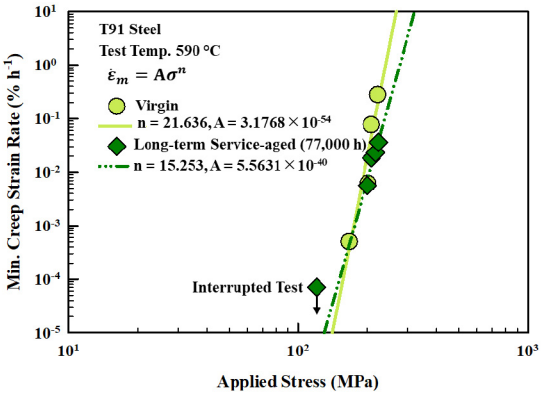

Fig. 4. Minimum creep strain rate versus applied stress for T91 steel at 590 °C.

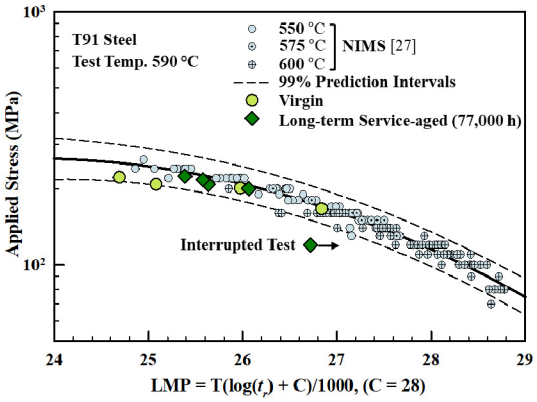

Fig. 5. Comparison of creep rupture life data of T91 steel measured at 590 °C: applied stress versus Larson-Miller parameter (LMP).

ing of grains, and precipitates along the lath martensitic boundary and PAGBs after long-term service.

The fracture surfaces of the creep-ruptured specimens under similar stress levels of 200.1-208.1 MPa were observed for the virgin and long-term service-aged materials, as shown in Fig. 6. The fracture surfaces of both materials were similar. The SEM images of the fracture surfaces for both creep-ruptured specimens showed ductile rupture features and consisted of several dimples as displayed in Figs. 6(a)-(d).

With the increase in the creep rupture times, the virgin and long-term service-aged materials exhibited a relatively low creep ductility trend; however, the overall trends of both materials displayed creep ductile failure with 86.32 % and 90.90 % reduction of areas, respectively (Table 2). The virgin and long-term service-aged materials showed average failure elonga-

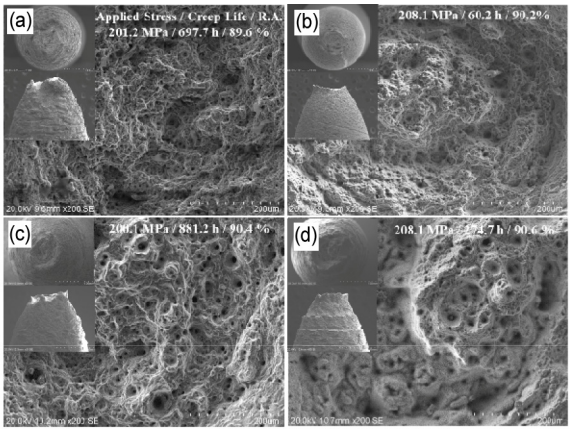

Fig. 6. Fracture surface of creep specimens: (a) and (b) virgin; (c) and (d) long-term service-aged (77000 h) T91 steel materials.

tions of 20.77 % and 22.88 %, respectively. The elongation trend indicated slight increase with increase in service time. The stress-enhanced recovery and coarsening of precipitates may lead to an increase in elongation with service time. However, both materials displayed similar creep ductility and failure elongation trends under similar applied stresses. Because the microstructural change due to precipitation for the long-term service-aged material is characterized by more fine precipitates within the grains and lath boundaries than those in the virgin material, this can lead to high creep strength in the long-term service-aged material.

3.2 Microstructural aging observation

The XRD patterns of the virgin and long-term service-aged specimens of T91 steel are illustrated in Fig. 7. Based on the JCPDS database, it was observed that martensite (JCPDS card no. 00-044-1290), $M_{23}C_6$ precipitate (JCPDS card no. 00-058-0762), and VN precipitate (JCPDS card no. 00-035-0768) were the main phases detected in both the virgin and long-term service-aged T91 materials.

Fig. 8 depicts the tempered martensite microstructures of the virgin and long-term service-aged materials, which were observed in OM images. The morphologies of residual δ-ferrite in the PAGB and lath boundary region can be seen in Fig. 8(a). A certain larger region of the residual δ-ferrite phase observed in the virgin material is considered to result in lower creep strength [2, 3]. Meanwhile, a small amount of residual δ-ferrite was present in the long-term service-aged material microstructure, as shown in Fig. 8(b). However, a few small dark precipitates within the small residual δ-ferrite were observed in Fig. 8(b), which were reported as MX precipitates with enriched V, Nb, N, and C [1, 3]. These small precipitates can reduce the effect of residual δ-ferrite in the long-term service-aged material. On the contrary, the larger amount of residual δ-ferrite phase observed in the virgin microstructure led to a lower hardness of the virgin material (225 HV) compared to that of the long-term service-aged material (231 HV). The negative

Table 4. Results of EDS analysis of the precipitates of the virgin and long-term service-aged (77000 h) T91 steel materials.

Specimen	Element	C	Si	Cr	Fe	V	Mo	Phase
Virgin	Pt. 1	5.13	-	-	76.94	15.96	1.97	MX
	Pt. 2	1.67	-	17.52	77.60	0.53	2.68	$M_{23}C_6$
Long-term service-aged (77000 h)	Pt. 3	1.14	0.68	-	75.80	18.72	3.66	MX
	Pt. 4	2.23	0.60	18.12	75.67	0.47	2.81	$M_{23}C_6$
	Pt. 5	-	0.79	20.46	69.76	-	8.99	Laves phase

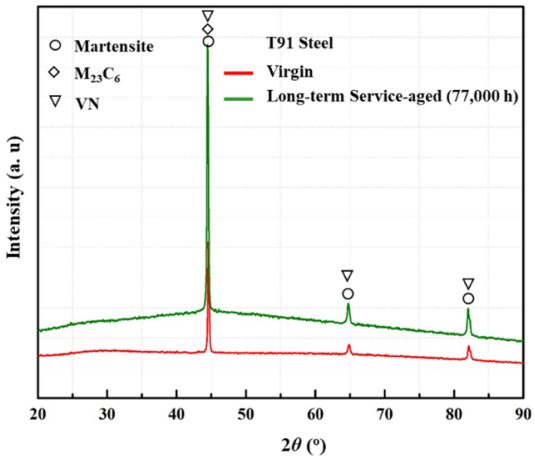

Fig. 7. XRD patterns of virgin and long-term service-aged (77000 h) T91 steel materials.

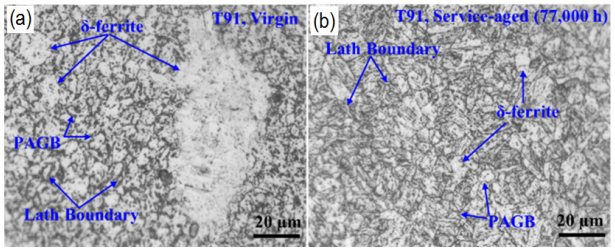

Fig. 8. Optical images of (a) virgin; (b) service-aged (77000 h) T91 steel materials at 590 °C.

effect of the δ-ferrite phase on the creep strength and toughness was also investigated in previous studies [3, 28-30]. However, the presence of the lath boundary in the microstructure of the virgin material and retention of the lath morphology in the long-term service-aged material was beneficial for blocking the effect of the dislocation movement [31].

Besides the effect of the initial microstructure, the formation of precipitates in both the virgin and long-term service-aged materials was an important factor influencing their creep rupture lives. Thus, FE-SEM/EDS and image analyses were also carried out to investigate the microstructure in more detail. Figs. 9(a) and (b) present the FE-SEM images of the microstructure of the virgin and long-term service-aged materials, respectively. Figs. 9(c) and (d) show higher magnifications of the area indicated by square in Figs. 9(a) and (b), respectively.

Precipitates distributed along the lath boundaries, grain

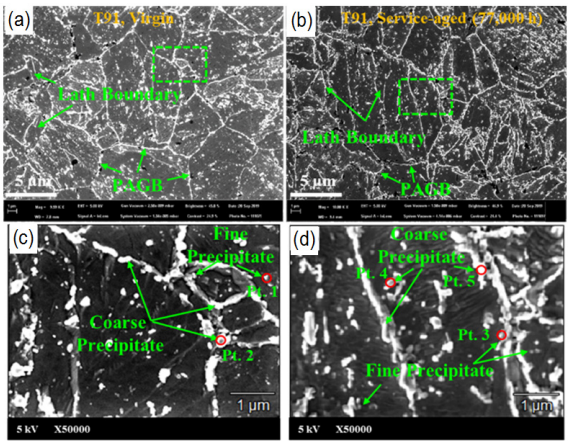

Fig. 9. FE-SEM images of (a) virgin; (b) service-aged (77000 h) T91 steel materials; (c) and (d) show the enlarged images of the area enclosed by the square in (a) and (b), respectively.

boundaries, and within grains were observed. There were two types of precipitate shapes: fine and coarse shapes. The results of FE-SEM and EDS analyses on each precipitate for the virgin and long-term service-aged materials are listed in Table 4. From the results of the FE-SEM/EDS and XRD analyses, the fine precipitates were an enrichment of V as the presence of MX precipitates (M = V, Nb and X = C, N), and the coarse precipitates were an enrichment of Cr as the presence of $M_{23}C_6$ precipitates (M = Fe, Cr, V, Mo). These identified precipitates were in good agreement with those in previous studies [1, 15, 32]. A new Laves phase $(Fe,Cr)_2Mo$ was formed in the long-term service-aged material with Fe, Cr, and Mo enrichments, which was also reported in previous studies [1, 11, 31, 33]. However, it is difficult to distinguish between two precipitates as the $M_{23}C_6$ and Laves phase, because these precipitates were observed along the grain boundaries and lath boundaries, as shown in Fig. 9(d). It should be noted that some black dots observed in Figs. 9(a) and (b) were due to the selection of in-lens signal for FE-SEM; however, the black dots could not be seen after the signal was changed from in-lens to backscattered electrons.

Further evidence verifying the formation of precipitates was obtained via FE-SEM and EDS mapping. Figs. 10(b)-(e) and (g)-(j) indicate that the EDS maps of elements C, N, Nb, and V, with an identical specimen region in Figs. 10(a) and (f), promote the formation of fine MX precipitates, which were mainly distributed within the grains and laths in both the virgin and

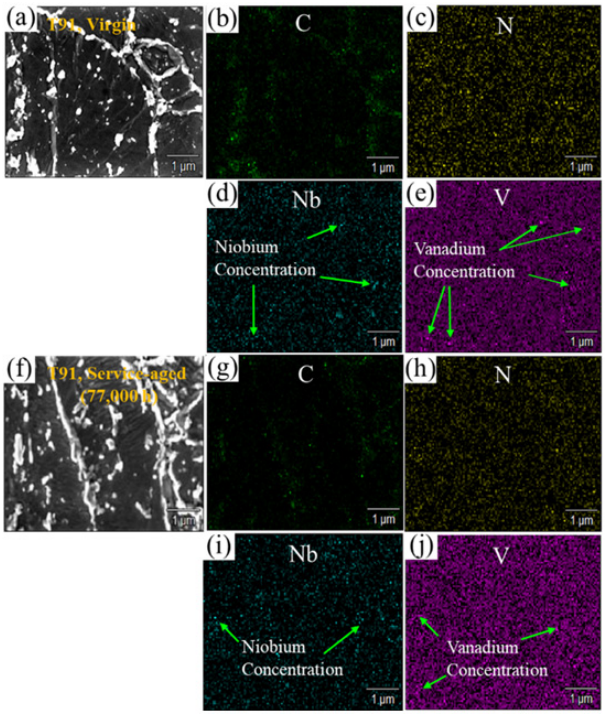

Fig. 10. FE-SEM images of the T91 steel to confirm MX precipitates: (b)-(e) EDS element mapping images corresponding to the (a) virgin material; (g)-(j) EDS element mapping images corresponding to the (f) service-aged (77000 h) material.

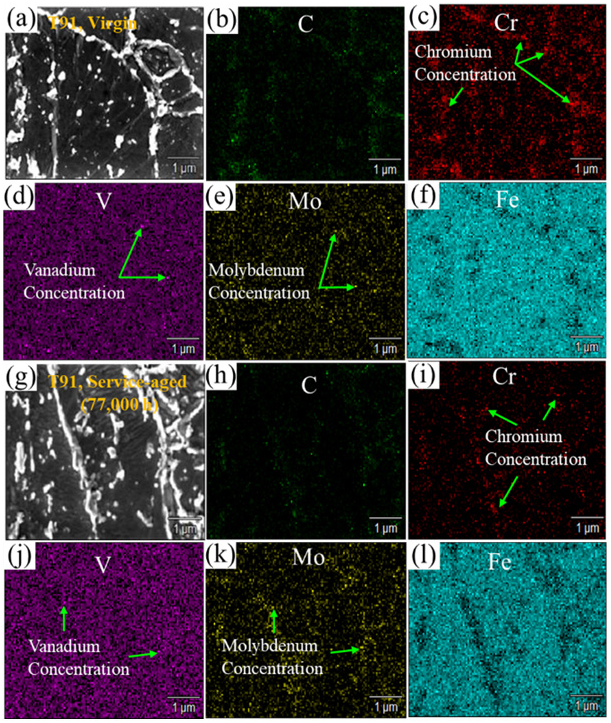

Fig. 11. FE-SEM images of the T91 steel to confirm $M_{23}C_6$ and Laves phase precipitates: (b)-(f) EDS element mapping images corresponding to the (a) virgin material; (h)-(l) EDS element mapping images corresponding to the (g) service-aged (77000 h) material.

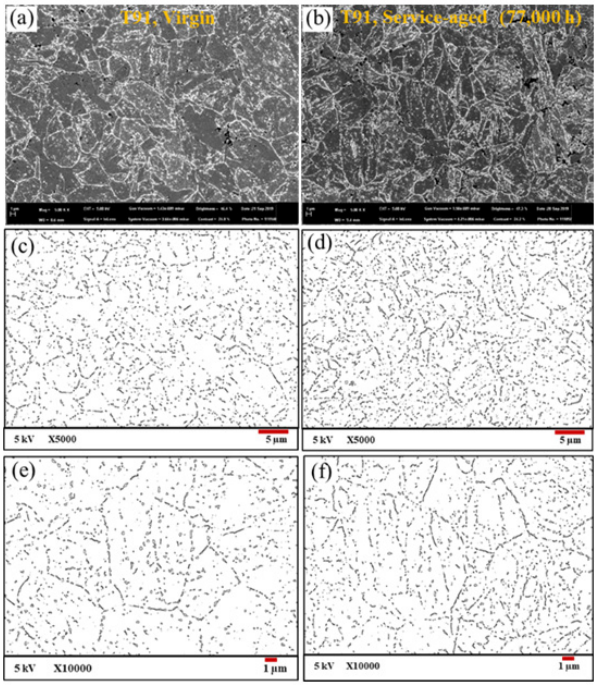

Fig. 12. FE-SEM images of precipitates in the (a) virgin; (b) service-aged (77000 h) materials. Images of precipitates after ImageJ post-processing for determining the number and size distribution of precipitates in the (c), (e) virgin; (d), (f) service-aged (77000 h) materials.

long-term service-aged materials, respectively. Meanwhile, the EDS maps of elements C, Cr, V, Mo, and Fe (Figs. 11(b)-(f) and (h)-(l)), with an identical specimen region in Figs. 11(a) and (g), respectively, promote the formation of $M_{23}C_6$ precipitates along the grain boundaries and lath boundaries. In addition, the formation of the Laves phase within the martensite laths and along various boundaries was revealed in the EDS maps of elements Cr, Mo, and Fe as displayed in Figs. 11(i), (k), and (l) for the long-term service-aged materials.

The main requirement for creep-resistant steels to be able to serve their purpose at elevated temperatures is high creep resistance. The enhancement in creep resistance is connected with stable precipitates that block the movement of dislocations and stabilize the sub-grain microstructure [16, 22, 34]. The presence of fine MX precipitates within the lath boundary resists the coarsening of lath, thereby increasing the creep strength during long-term service. However, if the service time is extended, the effects of fine precipitates can vanish, and the precipitates inside the grain become larger. Consequently, the grain also loses creep resistance. Thus, the creep resistance of the T91 steel observed in this study may be limited to a certain service time.

Besides the effect of fine precipitates on the creep resistance of T91 steel, the adding of V element in long-term service-aged T91 material to form Cr-rich multi-component mixed phase (Cr, Fe, V, Mo)$_{23}C_6$ which delayed or inhibited the coarsening of the $M_{23}C_6$–type of precipitate, which is similar to the research results of Li et al. [35] and Xu et al. [36]. Thus, $M_{23}C_6$ precipitates

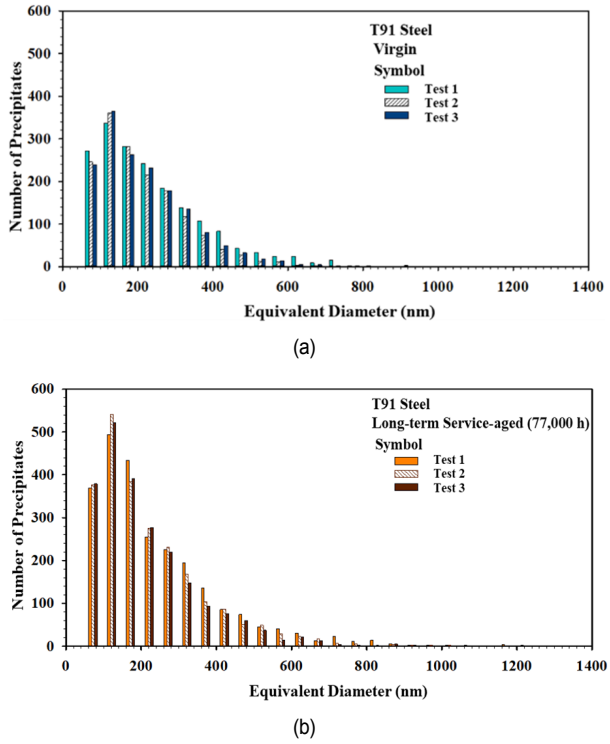

Fig. 13. Number and size distribution of precipitates in the (a) virgin; (b) long-term service-aged (77000 h) T91 steel materials at 590 °C.

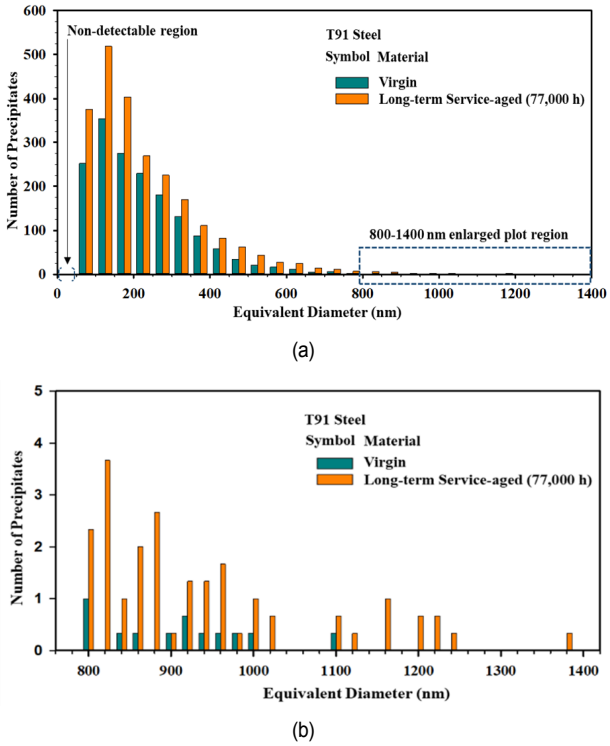

Fig. 14. Comparison of (a) number; (b) larger size of precipitates between the virgin and long-term service-aged (77000 h) materials at 590 °C.

show an equilibrium phase in T91 steel, which is responsible for long-term microstructural stability [37]. In fact, the precipitation of the Laves phase reveals a decrease in the amount of Mo in the solid solution, corresponding to a decrease in the creep resistance. However, the Laves phase precipitates have a positive influence on the enhancement of creep resistance, as a result of addition of B being contained in this material [15, 16, 38]. In addition, the Laves phase along the lath boundaries and grain boundaries can enhance the creep resistance by limiting the deformation of grains and laths for the long-term service-aged material [15].

Figs. 12(a) and (b) show the FE-SEM images of precipitates for the virgin and long-term service-aged materials, respectively. To indicate clearly the distribution of precipitates, high-magnification images in Figs. 12(c) and (e), (d) and (f), corresponding to Figs. 12(a) and (b), were captured and then binarized to carefully analyze the microstructure of the virgin and long-term service-aged materials, respectively. The number and average size distribution of precipitates in both the virgin and the long-term service-aged materials were measured based on binarized images with three locations presented as tests 1, 2, and 3 on the specimens, as illustrated in Fig. 13. The average number of precipitates from the three tests as indicated in Fig. 14(a) was increased by approximately 1670 and 2368 for the virgin and long-term service-aged materials, respectively. The average area fraction of precipitates from the three tests as indicated in Fig. 14(a) was 12.25 and 12.62 % for the virgin and long-term service-aged materials, respectively. The results showed the average area fraction of precipitates did not significantly change, but the average number of precipitates increased after 77000 h service. This means that the fine precipitated phases are continuously precipitated in the service 77000 h and the coarsening of larger precipitates is not significant. Also, the number of small precipitates less than 200 nm in size was higher in the long-term service-aged material (1298) than in the virgin material (882), as shown in Fig. 14(a). Thus, an increase in the number of precipitates of small sizes was observed after long-term service, which increased the creep rupture strength by pinning the dislocation movement of this material. However, owing to resolution limitation, the precipitates with equivalent diameters of less than approximately 50 nm were not detectable [15, 20]. In the virgin material, the maximum size of precipitates was approximately 1103 nm, while it increased to 1382 nm after long-term service (Fig. 14(b)). It was observed that the growth of precipitates was relatively slow even for long-term service. Thus, the stability of precipitate size and large amount of fine precipitates along grain boundaries, lath boundaries, and within the lath enhance the stability of the tempered martensite microstructure and lead to improvement of the creep rupture life during long-term service.

4. Conclusions

The characterization of the creep behavior of virgin and long-term service-aged T91 steel materials was established via

examination of the microstructure variations. These observations are limited for 77000 h serviced T91 material of this study. The following conclusions can be drawn from this study.

(1) The steel specimens displayed a decrease in creep ductility with an increase in rupture life in the low-stress regime.

(2) The creep rupture life of the virgin specimen was lower in the presence of δ-ferrite. On the contrary, the creep rupture life of the aged material benefitted from the formation of fine precipitates during long-term aging, in addition to the tempered martensite microstructure.

(3) The comparative assessment of the creep rupture strength of the T91 steel revealed that the age-induced degradation was negligible. The formation of fine precipitates such as MX, $M_{23}C_6$, and Laves phase had a beneficial effect on maintenance of the favorable mechanical properties throughout the long service period.

Acknowledgments

This work was supported by the KETEP (No. 2016 1110 100090), granted financial resource from the Ministry of Trade, Industry & Energy (MOTIE).

Nomenclature

A	: Creep coefficient
C	: Larson-Miller constant
LMP	: Larson-Miller parameter
n	: Creep exponent
T	: Temperature (K)
t_r	: Time to rupture (h)
σ	: Applied stress
$\dot{\varepsilon}$	: Creep strain rate

References

[1] V. T. Paul, S. Saroja and M. Vijayalakshmi, Microstructural stability of modified 9Cr-1Mo steel during long term exposures at elevated temperatures, *Journal of Nuclear Materials*, 378 (2008) 273-281.

[2] K. Kimura, K. Sawada, H. Kushima and Y. Toda, Influence of chemical composition and heat treatment on long-term creep strength of grade 91 steel, *Procedia Engineering*, 55 (2013) 2-9.

[3] S. Kobayashi, K. Sawada, T. Hara, H. Kushima and K. Kimura, The formation and dissolution of residual δ ferrite in ASME Grade 91 steel plates, *Materials Science and Engineering A*, 592 (2014) 241-248.

[4] EPRI, *Guidelines and Specifications for High-reliability Fossil Power Plants: 2nd Ed. Best Practice Guideline for Manufacturing and Construction of Grade 91 Steel Components*, Electric Power Research Institute, Palo Alto, California, US (2015).

[5] C. Pandey, N. Saini, M. M. Mahapatra and P. Kumar, Study of the fracture surface morphology of impact and tensile tested cast and forged (C&F) Grade 91 steel at room temperature for different heat treatment regimes, *Engineering Failure Analysis*, 71 (2017) 131-147.

[6] J. Baral, J. Swaminathan, D. Chakrabarti and R. N. Ghosh, Effect of welding on creep damage evolution in P91B steel, *Journal of Nuclear Materials*, 490 (2017) 333-343.

[7] J. Parker, Creep ductility considerations for high energy components manufactured from creep strength enhanced steels, *Materials at High Temperatures*, 34 (2) (2017) 109-120.

[8] A. B. Zala, N. I. Jamnapara, V. J. Badheka, S. Sam and M. Ranjan, Effect of aluminide coatings on penetration and microstructure of TIG welded 9Cr-1Mo steel for fusion blanket applications, *Fusion Engineering Design*, 144 (2019) 172-179.

[9] EPRI, *Guidelines and Specifications for High-reliability Fossil Power Plants, Best Practice Guideline for Manufacturing and Construction of Grade 91 Steel Components*, Electric Power Research Institute, Palo Alto, California, US (2011).

[10] W. G. Kim, J. Y. Park, M. G. Won, H. Y. Lee and N. S. Huh, Non-linear modeling of stress relaxation curves for Grade 91 steel, *Journal of Mechanical Science and Technology*, 32 (2018) 1143-1151.

[11] A. Grybėnas, V. Makarevičius, A. Baltušnikas, I. Lukošiūtė and R. Kriūkienė, Correlation between structural changes of $M_{23}C_6$ carbide and mechanical behaviour of P91 steel after thermal aging, *Materials Science and Engineering A*, 696 (2017) 453-460.

[12] R. Viswanathan, J. Sarver and J. M. Tanzosh, Boiler materials for ultra-supercritical coal power plants-steamside oxidation, *Journal of Materials Engineering and Performance*, 15 (3) (2006) 255-274.

[13] T. Gheno, D. Monceau, J. Zhang and D. J. Young, Carburisation of ferritic Fe-Cr alloys by low carbon activity gases, *Corrosion Science*, 53 (2011) 2767-2777.

[14] EPRI, *The Benefits of Improved Control of Composition of Creep Strength Enhanced Ferritic Steel Grade 91*, Electrical Power Research Institute, Palo Alto, California, US (2014).

[15] S. Fetni, A. Toumi, I. Mkaouar, C. Boubahri and J. Briki, Microstructure evolution and corrosion behaviour of an ASTM A213 T91 tube after long term creep exposure, *Engineering Failure Analysis*, 79 (2017) 575-591.

[16] G. Golański, A. Zielińska-Lipiec, A. Zieliński and M. Sroka, Effect of long-term service on microstructure and mechanical properties of martensitic 9% Cr steel, *Journal of Materials Engineering and Performance*, 26 (3) (2017) 1101-1107.

[17] *ASTM E139-11, Standard Test Methods for Conducting Creep, Creep-rupture, and Stress-rupture Tests of Metallic Materials*, American Society for Testing and Materials, West Conshohocken, PA 19428-2959, US (2018).

[18] V. H. Dao, J. S. Song, J. Y. Kim and K. B. Yoon, Creep deformation characteristics of microalloyed HP40Nb steel at 950 °C, *Journal of Mechanical Science and Technology*, 33 (10) (2019) 4813-4821.

[19] T. G. Le, K. B. Yoon and T. M. Jeong, Degradation and reduction of small punch creep life of service-exposed Super304H steel, *Journal of Mechanical Science and Technology*, 33 (11) (2019) 5243-5250.

[20] Q. Xiong, J. D. Robson, L. Chang, J. W. Fellowes and M. C. Smith, Numerical simulation of grain boundary carbides evolution in 316H stainless steel, *Journal of Nuclear Materials*, 508 (2018) 299-309.

[21] C. Dethloff, E. Gaganidze and J. Aktaa, Quantitative TEM analysis of precipitation and grain boundary segregation in neutron irradiated EUROFER 97, *Journal of Nuclear Materials*, 454 (2014) 323-331.

[22] C. G. Panait, A. Z. Lipiec, T. Koziel, A. C. Filemonowicz, A. F. G. Lorenzon and W. Bendick, Evolution of dislocation density, size of subgrains and MX-type precipitates in a P91 steel during creep and during thermal ageing at 600°C for more than 100,000h, *Materials Science and Engineering A*, 527 (2010) 4062-4069.

[23] ASTM E2578-07, *Standard Practice for Calculation of Mean Sizes/diameter and Standard Deviations of Particle Size Distribution*, American Society for Testing and Materials, West Conshohocken, PA 19428-2959, US (2018).

[24] ASTM E647-15, *Standard Test Method for Measurement of Fatigue Crack Growth Rates*, American Society for Testing and Materials, West Conshohocken, PA 19428-2959, US (2015).

[25] K. Guguloth and N. Roy, Creep deformation behavior of 9Cr1MoVNb (ASME Grade 91) steel, *Materials Science and Engineering A*, 680 (2017) 388-404.

[26] T. Shrestha, M. Basirat, I. Charit, G. P. Potirniche, K. K. Rink and U. Sahaym, Creep deformation mechanisms in modified 9Cr-1Mo steel, *Journal of Nuclear Materials*, 423 (2012) 110-119.

[27] NIMS, *Creep Datasheet No. 43A*, Data sheets on the elevated temperature properties of 9Cr-1Mo-V-Nb steel tubes for boilers and heat exchangers (ASME SA-213/SA-213M Grade T91), 9Cr-1Mo-V-Nb steel plates for boilers and pressure vessels (ASME SA-387/SA-387M Grade 91) and 9Cr-1Mo-V-Nb steel seamless pipe high temperature service (ASME SA-335/SA-335M Grade P91), National Institute for Materials Science (NIMS) (2014).

[28] K. Maruyama, K. Sawada and J. I. Koike, Strengthening mechanisms of creep resistant tempered martensitic steel, *ISIJ International*, 41 (6) (2001) 641-653.

[29] M. W. Kuper and B. T. Alexandrov, Retention of delta ferrite in the heat-affected zone of grade 91 steel dissimilar metal welds, *Metallurgical and Materials Transactions A*, 50A (2019) 2732-2747.

[30] C. Pandey, M. M. Mahapatra, P. Kumar and N. Saini, Comparative study of autogenous tungsten inert gas welding and tungsten arc welding with filler wire for dissimilar P91 and P92 steel weld joint, *Materials Science and Engineering A*, 712 (2018) 720-737.

[31] C. Pandey, M. M. Mahapatra, P. Kumar, R. S. Vidyrathy and A. Srivastava, Microstructure based assessment of creep rupture behaviour of cast forged P91 steel, *Materials Science and Engineering A*, 695 (2017) 291-301.

[32] J. M. Yu, V. H. Dao, V. Lok, T. G. Le and K. B. Yoon, Asymptotic creep deformation behavior of modified HP steel after long-term service, *Journal of Mechanical Science and Technology*, 34 (5) (2020) 1997-2009.

[33] A. Kipelova, A. Belyakov and R. Kaibyshev, Laves phase evolution in a modified P911 heat resistant steel during creep at 923K, *Materials Science and Engineering A*, 532 (2012) 71-77.

[34] G. Golański, A. Zielińska-Lipiec, S. Mroziński and C. Kolan, Microstructural evolution of aged heat-resistant cast steel following strain controlled fatigue, *Materials Science and Engineering A*, 627 (2015) 106-110.

[35] Y. Li, J. Du, L. Li, K. Gao, X. Pang and A. A. Volinsky, Mechanical properties and phases evolution in T91 steel during long-term high-temperature exposure, *Engineering Failure Analysis*, 111 (2020) 104451.

[36] Y. Xu, X. Zhang, Y. Tian, C. Chen, Y. Nan, H. He and M. Wang, Study on the nucleation and growth of $M_{23}C_6$ carbide in a 10% Cr martensite ferritic steel after long-term aging, *Materials Characterization*, 111 (2016) 122-127.

[37] C. Pandey, S. Sirohi, M. M. Mahapatra, P. Kumar and K. K. Bansal, Role of heat treatment on grain refinement and microhardness of 9Cr-1Mo-V-Nb steel, *Metallography, Microstructure, and Analysis*, 8 (2019) 472-478.

[38] E. Plesiutschnig, C. Beal, S. Paul, G. Zeiler and C. Sommitsch, Optimised microstructure for increased creep rupture strength of MarBN steels, *Materials at High Temperatures*, 32 (3) (2015) 318-322.

Vanno Lok received his B.S. in Industrial and Mechanical Engineering from Institute of Technology of Cambodia. He received M.S. in Mechanical Engineering from Chung-Ang University. He is currently a Ph.D. candidate in Chung-Ang University. His research interests are stress analysis problem in pressure vessel & piping application in power plant and microstructural analysis of high temperature fracture mechanics to structural materials in life assessment.

Thi Giang Le received her B.S. in Metallurgical Engineering from Hanoi University of Science and Technology. She received M.S and Ph.D. in Mechanical Engineering from Chung-Ang University. Her research interest is creep behavior and aging characteristics of the high temperature alloy materials.

Jong Min Yu received his M.S. in Mechanical Engineering from Chung-Ang University. He is currently a Ph.D. candidate in Chung-Ang University. His research interest is life and integrity assessment of facilities in power and process plants. He is also interested in creep fracture of additive manufactured components.

Young Wha Ma received his Ph.D. degree in Mechanical Engineering from Chung-Ang University, Korea in 2007. After that, he worked at Georgia Institute of Technology, U.S.A. as a postdoc. Dr. Ma is currently Senior Research Engineer at Doosan Heavy Industries & Construction. His research interest is application of high temperature fracture mechanics to residual life assessment of structural materials including single and directionally solidified superalloys such as gas turbine blade.

Vinh Phu Nguyen received his B.S. degree in Material Technology from Bach Khoa University, Ho Chi Minh City, Vietnam, in 2014, and M.S. degree in Mechanical Engineering from University of Ulsan, Ulsan, Korea. In 2016 he joined and is currently Ph.D. candidate at Chung-Ang University. His research fields are molecular dynamics, fracture mechanics and high temperature creep deformation.

Seung Tae Choi received his Ph.D. degree from Korea Advanced Institute of Science and Technology. He is currently a Professor at Chung-Ang University. His current research interests include multiscale analysis of deformation and fracture of polycrystalline materials and development of ferroelectric polymer sensors and actuators.

Kee Bong Yoon received his B.S. in Mechanical Engineering from Seoul National University, M.S. from KAIST and Ph.D. from Georgia Institute of Technology. He is currently a Professor at Chung-Ang University. His research interests are high temperature fracture and risk based management of energy plants and semiconductor plants. He is extending research to fracture of additive manufactured materials.